Effect of Ni Content on the Structural and Electrochemical Properties of $Mg_{1.9}Cu_{0.1}Ni_\chi$ alloys

Z.G. Huang*, Z.P. Guo, H.K. Liu, S.X. Dou

Institute for Superconducting and Electronic Materials, University of Wollongong, New South Wales 2522, Australia

Abstract: *Mg-based alloys, $Mg_{1.9}Cu_{0.1}Ni_\chi$ (χ = 1.8, 1.9, 2.0, 2.1), were fabricated through high-energy ball milling, and the effects of nickel content on the electrochemical characteristics have been investigated. A high discharge capacity of 490 mAhg^{-1} was observed for χ = 1.8, compared with 435 mAhg^{-1} for χ = 2.1. As to capacity degradation, 66.7 % of initial capacity was lost after 15 cycles for χ = 1.8, while only 47.2 % for χ = 2.1. Cyclic Voltammograms (CV) indicates that nickel can help maintain redox reaction current and consequently improve the cycle performance. The X-ray mapping analysis indicates that Mg, Ni, and Cu are uniformly distributed in the particles. The O content in the alloy electrodes after 15 cycles decreases with the increase of Ni content in the alloys, suggesting that Ni can efficiently suppress the formation of $Mg(OH)_2$. The linear polarization curves show that the exchange current density, namely the rate of hydriding/dehydriding, increases from 13 mAg^{-1} to 133 mAg^{-1} when the nickel content varies from 1.8 to 2.1. This is also considered as a reason for the observed improved capacity stability.*

Key words : hydrogen storage, Mg-based alloys, mechanical alloying, electrochemical properties

1. INTRODUCTION

Magnesium-based alloys have attracted many scientists' and technologists' attention, because they are potentially the most important candidates for hydrogen storage [1-10]. However, they can only absorb hydrogen at a relatively high temperature and with a slow kinetics, which has limited their applications. At present, there are basically two kinds of methods applied to improve the absorption/desorption kinetics: 1) substitution of Mg or Ni with other metal elements; 2) mechanical alloying to get amorphous or nanocrystalline Mg-based alloy [4]. Many experiments have proved that amorphous or nanocrystalline alloys can greatly improve the kinetics of hydriding/dehydriding because these alloys possess more active sites for hydrogen absorption and desorption, and accelerate the hydrogen diffusion in the alloys compared with bulk crystalline alloys [1~4]. Currently all the experiments aim to find a way to increase the number of active sites for absorption/desorption of hydrogen. In

practice the adjustment of the alloy particle surface is very important to improve the rate of absorption/desorption. Mechanical alloying (MA) is a kind of solid-state reaction by continuous mechanical collisions between balls and powders. Numerous structural defects and strains in the lattice are induced, and all these defects and grain boundaries introduced by the repeated breaks and cold welding of the powder act as active sites for hydrogen absorption and desorption [11, 12, 13]. It is well known that Ni has good electrochemical catalysis and electronic conductivity [14, 15, 16], and several authors have reported that nickel has excellent catalytic activity during the hydrogen storage process [14-19]. S. Nohara et al. achieved a maximum discharge capacity of 870 mAhg^{-1} for Mg_2Ni ball milled with 30 % Ni [19], which is almost up to the theoretical capacity of 999 mAhg^{-1} [8]. H. Inoue et al. found that Ni can greatly improve the high rate discharge ability and cycle performance of $Mg_{0.9}Ti_{0.06}V_{0.04}Ni_\chi$ (χ = 1.0,1.1,1.2,1.3) [17]. S.G. Zhang et al. [20] suggested that the Ni-enriched layer under the top surface of Mg-based alloy facilitates the hydriding and dehydriding, while others [21] found that Ni was very effective in

---

*To whom correspondence should be addressed: Fax: 61 2 4221 3712, email: zh104@uow.edu.au

protecting the electrode surface from oxidation, which consequently improves the cycle performance. Similarly, Cu can also act as a catalyst for the absorption and dissociation of hydrogen molecules. In hydrogen storage alloys, Cu substituted alloy shows an obvious improvement in the reaction rate and a decreased working temperature. These alloys have been investigated by many researchers [22, 23, 24, 25, 26].

Based on the above information, we chose mechanical alloying as the fabrication method to obtain alloys of $Mg_{1.9}Cu_{0.1}Ni_{\chi}$, with nickel in the composition varying from $\chi = 1.8$ to 2.1. The electrochemical performance of many Mg-based alloys has been reported before. However, to our knowledge there have been few investigations on Mg-Cu-Ni alloy electrodes. A series of measurements have been conducted in order to find the relationship between structural characteristics and electrochemical properties in terms of nickel content.

2.   EXPERIMENTAL DETAILS

Pure (purity greater than 99.9 %) metal elemental powders of Mg, Ni and Cu were weighed out according to the atomic ratio. The mechanical milling was carried out using a Spex 8000 Mixer Mill, with a weight ratio of balls to powder of 10:1. The stainless steel jar was sealed with a rubber O ring and filled with argon in a glove box before operation. The concentrations of oxygen and water in the argon were below 10 ppm according to the oxygen and water detectors in the glove box. Because of the severe cold welding during ball milling, especially for high energy milling, after each 99 minutes the jar was cleaned, and any bulk materials were crushed into powder using a mortar, ensuring that all three elements were fully mixed together and that the composition was uniform. The whole duration of the milling was 10 h. Four alloy samples were prepared with the following compositions: $Mg_{1.9}Cu_{0.1}Ni_{1.8}$, $Mg_{1.9}Cu_{0.1}Ni_{1.9}$, $Mg_{1.9}Cu_{0.1}Ni_{2.0}$, $Mg_{1.9}Cu_{0.1}Ni_{2.1}$.

X-ray diffraction (XRD) spectra of the milled powders were recorded with Philips PW 1730 and Siemens D 500 diffractometers using Cu Kα radiation ($\lambda = 0.15418$ nm) at operating parameters of 20 mA, 40 kV, step size 0.05 ^{o} and speed 2 ^{o} / min. The particle morphology was characterized through Analytical Scanning Electron Microscopy (JEOL, JSM-6460A) equipped with Energy Dispersive X-ray Spectrometry (EDS). The distribution of Mg, Ni, Cu and O in the alloy was investigated through EDS mapping. Alloy particle sizes and size distribution were determined by a MALVERN Particle Size Analyser.

The alloy powder was mixed with nickel powder according to a mass ratio of 1:2. The mixture was first made into slurry with addition of 5% PVA solution, then the slurry was pasted onto a nickel foam, which acts as the current collector for the negative electrode. After being pressed, the electrode was wrapped with a non-woven fabric separator. A $NiOOH/Ni(OH)_2$ electrode was selected as the counter electrode and 6 M KOH as the electrolyte. The charge and discharge properties of the Mg-based alloy as negative electrode were measured with a DC-5 battery tester controlled by a computer at room temperature. The electrode was charged at 100 mAg^{-1} for 10 h and discharged at 20 mAg^{-1} with a cut-off voltage of 0.900 V. Linear polarization, Cyclic Voltammetry (CV) and a.c impedance measurements were performed using a CHI660B electrochemical workstation. Three electrode system was used with Hg/HgO as the reference electrode and $NiOOH/Ni(OH)_2$ as the counter electrode. The apparent surface area of the electrode was 1 cm^2.

3.   RESULTS AND DISCUSSION

Figure 1 shows the X-ray diffraction patterns of the high energy ball milled Mg-based alloys. It is clear that all the ball milled alloys are amorphous, with only a broad peak visible, which is characteristic of the amorphous MgNi structure [1, 17, 27]. No peaks corresponding to Cu and Ni exist, implying that the copper and nickel atoms were dissolved in the Mg-based alloy without changing its structure significantly. This indicates that in the present low nickel content range the kinetics of amorphization by ball milling of MgNi is not changed. However, there is a minor change in the XRD patterns as the Ni content varies from 1.8 to 2.1. The XRD band position shifts to a higher angle as the Ni content increases in the alloys, which is due to the smaller atomic diameter of Ni compared with that of Mg [20].
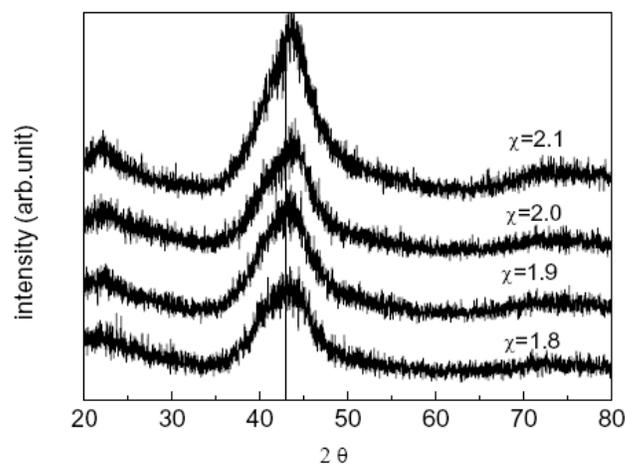

Figure 1:   X-ray diffraction patterns of ball-milled $Mg_{1.9}Cu_{0.1}Ni_{\chi}$ (χ = 1.8, 1.9, 2.0, 2.1) alloys.

Figure 2 is a SEM image of the as-received alloy ($Mg_{1.9}Cu_{0.1}Ni_{1.9}$) powder and Mg, Ni, Cu and O distribution in the alloy. All the other alloy powders with different Ni content have similar morphology to this and are not shown here.

The characteristics of products of mechanical alloying are obviously seen in this picture. Ball milling constantly creates fresh surfaces during the process as a result of repeated cold-welding and fracturing. Fragments created by collisions are cold welded together again by impacts and form irregular particles with the edges left behind. From the EDS mapping, all the elements, including the oxygen impurity, which was introduced from the raw materials and / or leaking of the milling jar, are homogenously distributed, without any agglomeration, which means that the high energy ball milling is an effective way to obtain the alloy. Considering the XRD patterns shown in Figure 1, it is obvious that Cu and additional Ni atoms have dissolved in the MgNi amorphous alloy without greatly changing its structure [1, 17, 27], which implies that through high energy ball milling amorphous alloy can be fabricated with homogenous microstructure. The particle size varies from several microns to several tens of microns as observed from the Particle Size Analyzer, and more than fifty percent of the particles are about 5 microns, which is regarded as the mean particle size.
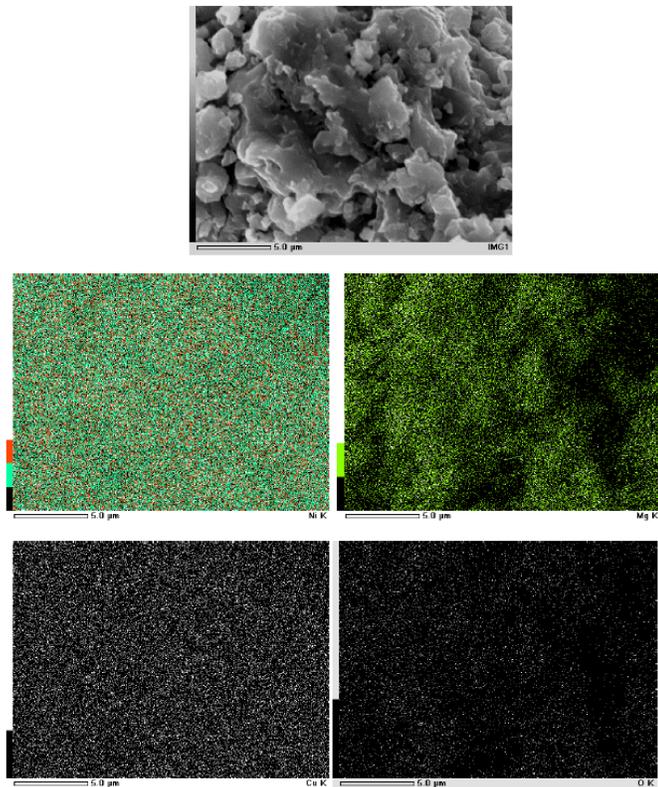

Figure 2: SEM image of as-received $Mg_{1.9}Cu_{0.1}Ni_{1.9}$ alloy and Mg, Ni, Cu and O distribution in the alloy.

Discharge capacities as a function of cycle number for the $Mg_{1.9}Cu_{0.1}Ni_\chi$ (χ = 1.8, 1.9, 2.0, 2.1) electrodes are shown in Figure 3. As a comparison, the capacity of MgNi amorphous

alloy fabricated by the same method in our lab was also shown in the Figure. The maximum discharge capacities, 490 mAhg^{-1} for χ = 1.8 and 435 mAhg^{-1} for χ = 2.1 were observed at the first cycle. The discharge capacity decreased during the subsequent cycles for all the four electrodes. However, the degradation of capacity increased as the nickel content in the alloys decreased. As for the electrode with χ = 1.8, after 15 cycles the discharge capacity is approximately only 150 mAhg^{-1}, compared to 250 mAhg^{-1} for χ = 2.1 after the same number of cycles. Evaluated from the percentage of degradation, that is $(C_1-C_{15})/C_1$, where C_1 represents the first discharge capacity and C_{15} is the capacity at the 15th cycle, the capacity decays was 66.7 %, 59.1 %, 57.1 %, 47.2 % with increasing Ni content from 1.8 to 2.1. Clearly, an increase in Ni content in the alloys can greatly enhance the cycle performance of the negative electrodes. As for MgNi, the maximum capacity is almost the same as that of the alloy electrode with χ = 2.1, but the percentage of degradation is 57.9 %, still quite high. Since Cu contributes little to the improvement of cycle performance [23, 24, 25], it is obvious that Ni plays a major role in the cycle stability.
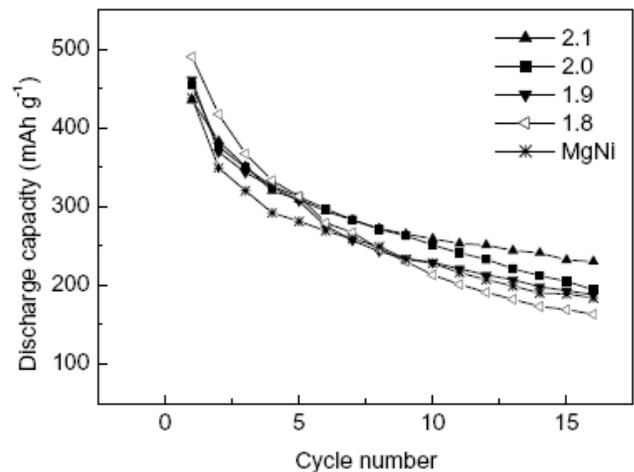

Figure 3: Discharge capacity via cycle number for $Mg_{1.9}Cu_{0.1}Ni_\chi$ (χ = 1.8, 1.9, 2.0, 2.1) and MgNi alloy negative electrodes.

Figure 4 shows the Cyclic Voltammograms of χ = 1.9 before charge and after 5 cycles at room temperature. It shows a large redox reaction current density associated with hydrogen absorption and desorption before cycling. The current density decreases after five cycles, indicating that the number of active sites for hydrogen absorption and desorption in the alloys decrease during the subsequent cycles. The first CV observations of amorphous MgNi as negative electrode were reported by T. Abe [6] using a special micropaste electrode technique. The shapes of the CV curves they got are different from the ones in this paper, although the potentials at i = 0 are similar. Because

the working electrode they used was made by packing MgNi powder into a concave area in a tungsten metal bar with a diameter of 1mm, and the scan rate they used was 1 mV/s instead of 10 mV/s, the polarization should be much smaller than that in our experiment. According to other reports [28-31], the degradation of capacity is due to the corrosion of Mg, which forms $Mg(OH)_2$. The irreversible reaction has two results: a) reduction of the amount of active Mg metal atoms in the alloy, which play a major role during the hydrogen uptake and release; b) formation of a shield which blocks the diffusion of hydrogen from the bulk to the surface and in the opposite direction, thereby increasing the activation energy during the absorption and desorption.
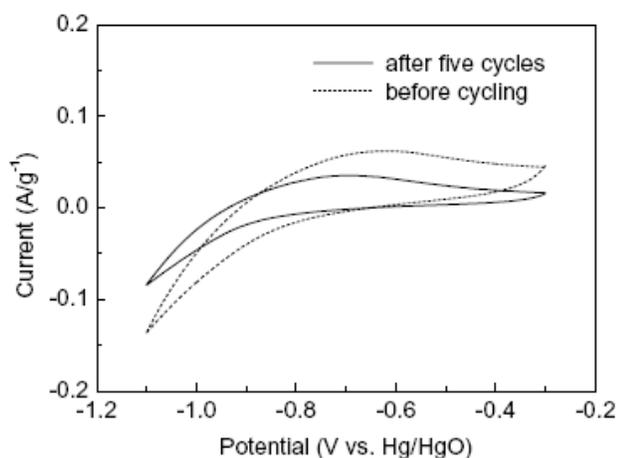

Figure 4: Cyclic Voltammograms of $Mg_{1.9}Cu_{0.1}Ni_{1.9}$ alloy electrode. Scan rate: 10 mV/s

Figure 5 shows the SEM image and concentration distributions of Mg, Ni, Cu and O in $Mg_{1.9}Cu_{0.1}Ni_{1.9}$ after five cycles. All the other electrode powders also have similar morphology and are not shown here. It is clear that there are many O atoms homogeneously distributed in the alloy ($Mg_{1.9}Cu_{0.1}Ni_{1.9}$). Because Mg is much more easily oxidized than Ni, most of the O atoms should combine with Mg, which means that the Mg has been severely oxidized during cycling. Once oxidized, Mg loses the ability to absorb hydrogen. This verifies the above explanation of the cycle performance degradation. This figure also shows a uniform distribution of Mg, Cu and Ni in the alloy, which means that no elemental agglomeration occurs during hydrogen absorption and desorption. Another point that needs to be pointed out is the morphology of the particles has changed after 5 charge/discharge cycles. There are some obvious edges in the as-prepared alloy particles (in Figure 2), while the particles become round after several charge/discharge cycles. This is probably due to the reaction priority that atoms in the edges are first to react. Ma [28] reports the formation of a dense corrosion layer on MgNi powder after immersion in alkaline electrolyte

solution, but no appreciable content of $Mg(OH)_2$ was found after MgNi was ball milled with Pd, and this modification greatly improves the cycle performance. In this experiment, EDS results show that the O concentration in the electrodes decreases as Ni content in the alloy increases, which means that the formation of $Mg(OH)_2$ is inhibited. Consequently the discharge capacity of an electrode with more Ni is kept comparatively high for many cycles.
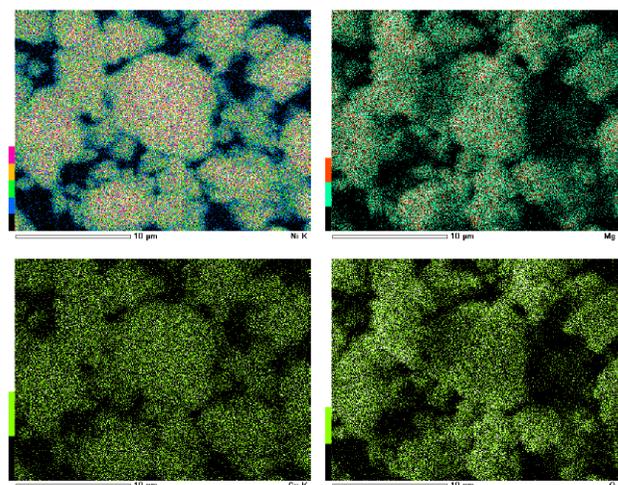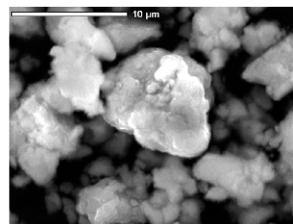

Figure 5: SEM image and concentration distributions of Mg, Ni, Cu and O in $Mg_{1.9}Cu_{0.1}Ni_{1.9}$ after five cycles.

Figure 6 shows the Cyclic Voltammograms of the alloys after 5 cycles. It is clear that the electrodes with higher nickel contents have a higher current density, which means that there are more active sites for hydrogen absorption/desorption after cycling when the nickel content is higher, and consequently the cyclic capability is improved from $\chi = 1.8$ to $\chi = 2.1$. According to other research [20], there is a Ni enriched layer underneath the top surface of the alloy. The Ni enriched layer near the surface of the alloy acts as a protective shield for the elemental Mg, which means that Ni can suppress the formation of $Mg(OH)_2$ and improve the cyclic stability. The results of charge–discharge experiments also support this conclusion.

Figure 7 illustrates the electrochemical impedance spectra (EIS) of the alloy electrodes at 80 % depth of discharge after 15 cycles. It has been suggested [32] that the semicircle in the high frequency region is characteristic of the charge-transfer process
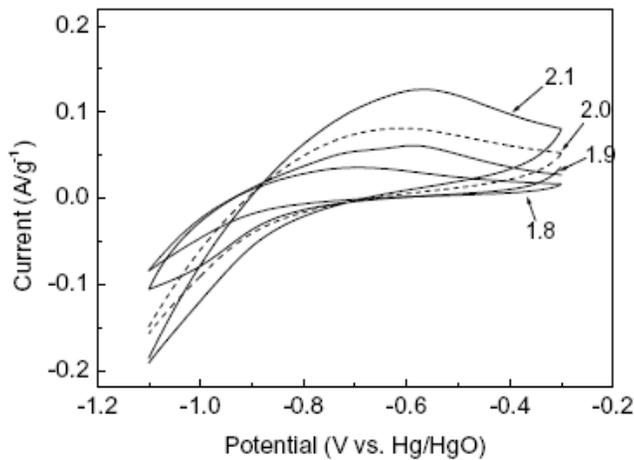
Figure 6: Cyclic Voltammograms for Mg$_{1.9}$Cu$_{0.1}$Ni$_\chi$ (χ = 1.8, 1.9, 2.0, 2.1) alloy electrodes after 5 cycles. Scan rate: 10 mV/s
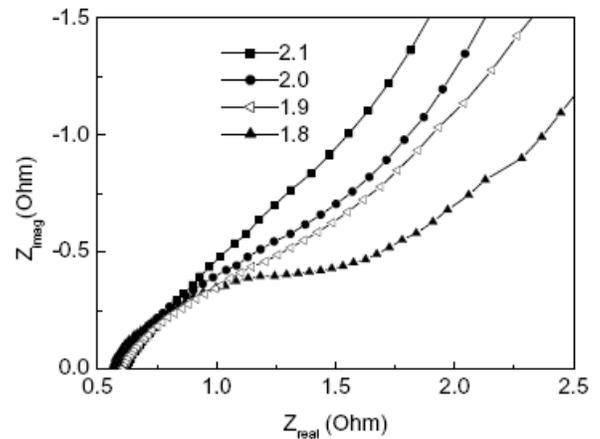

Figure 7: Electrochemical impedance spectra of Mg$_{1.9}$Cu$_{0.1}$Ni$_\chi$ (χ = 1.8, 1.9, 2.0, 2.1) alloy electrodes after 15 cycles at 80 % depth of discharge.

at the alloy/electrolyte interface, and the linear response in the low frequency region is indicative of hydrogen diffusion in a bulk alloy. When the depth of discharge is above 70 %, there will be a fast charge-discharge process and slow diffusion of hydrogen in the alloy electrode [13, 14] because of the low hydrogen concentration in the metal hydride electrode. So the rate-determining process should be hydrogen diffusion when the depth of discharge is 80 %. However, as can be seen from the impedance spectra, there is still a semicircle. Considering the electrode state, i.e. 80 % depth of discharge after 15 cycles, we believe that the semicircle is due to the passivation layer on the electrode surface [33, 34]. With Ni content increasing, the semicircle in the high-frequency region become smaller and even disappears. This might be ascribed to: 1) the high electrocatalytic activity owing to the higher concentration of Ni; 2) passivation suppression on the electrode surface caused by the higher content of Ni.

The exchange current density I_o was determined from the linear polarization curves [11]. The linear polarization curves were obtained at 1 mV/s at a small overpotential versus the stabilized open circuit potential. Figure 8 shows the linear polarization curves of the alloy electrodes at 20 % depth of discharge after 15 cycles. Obviously there is a good linear dependence of the polarization current at small overpotential (20 mV). The exchange current density I_o can be calculated according to the linearized form of the Butler–Volmer equation, which is valid at low overpotentials [35]:

$$I = I_o F \eta / RT \qquad (1)$$

where R is the gas constant, T the absolute temperature, F the Faraday constant, and η is the overpotential. The calculated val-
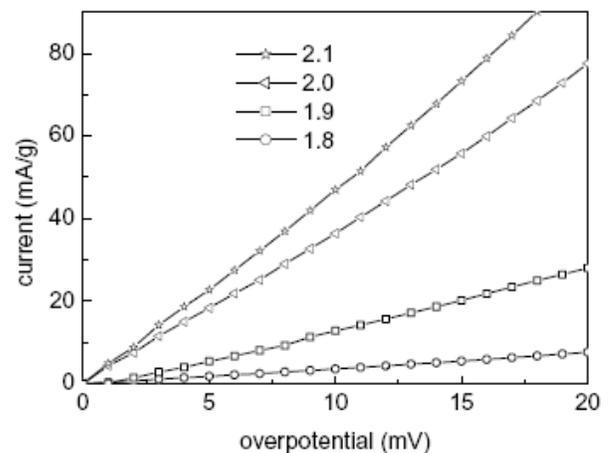

Figure 8: Linear polarization curves of Mg$_{1.9}$Cu$_{0.1}$Ni$_\chi$ (χ = 1.8, 1.9, 2.0, 2.1) alloy electrodes after 15 cycles at 20 % depth of discharge.

ues of the exchange current densities are illustrated in Figure 9. As is well known, exchange current density I_o is an important kinetic parameter for the charge/discharge reaction. It represents the rate of hydriding/dehydriding, from which reversibility and discharge capacity can be evaluated. As can be seen from Figure 9, with increasing Ni content, the exchange current density increases from 13 mAg^{-1} to 133 mAg^{-1}. It is well known that nickel has excellent electrocatalytic activity and electronic conductibility [14, 15, 16]. Therefore, the electrocatalytic activation of the electrodes increases with increasing Ni content, resulting in an increase of I_o. Combining this with the EIS spectra and discharge curves, it is evident that the Ni can reduce the resistance of the hydriding/dehydriding process, which consequently helps to improve the cycle performance.
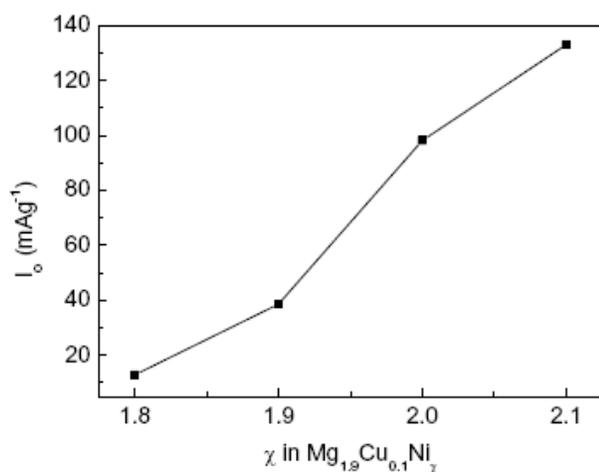

Figure 9: Variation of exchange current density with χ in $Mg_{1.9}Cu_{0.1}Ni_{\chi}$.

4.   CONCLUSION

The effect of nickel content on the electrochemical properties of $Mg_{1.9}Cu_{0.1}Ni_{\chi}$ (χ = 1.8, 1.9, 2.0, 2.1) hydrogen storage alloys has been reported in this paper. Although the initial discharge capacity of the alloy electrodes with higher Ni content is slightly lower, the capacity decays are 66.7 %, 59.1 %, 57.1 %, 47.2 % with increasing Ni content from χ = 1.8 to χ = 2.1. Clearly nickel can reduce the extent of discharge capacity degradation. The improvement of the electrochemical performance can be explained by the following facts: (1) the high electrocatalytic activity of Ni in alloys; (2) the suppression of the formation of $Mg(OH)_2$ on the surface of electrodes; (3) the high rate of absorption and desorption of hydrogen, as evidenced by the exchange current density, which increases almost ten times to 133 mAg^{-1} when χ = 2.1.

REFERENCES

[1] L. Sun, G.X. Wang, H.K. Liu, D.H. Bradhurst, S.X. Dou, Electrochem. Solid-State Lett., 3, 121 (2000).

[2] N.H. Goo, W.T. Jehong, K.S. Lee, J. Power Sources, 87, 118 (2000).

[3] S. Ruggeri, L. Roue, J. Power Sources, 117, 260 (2003).

[4] H.K. Liu, Encyclopedia of Nanoscience and Nanotechnology, 4, 775 (2004).

[5] D. Mu, Y. Hatano, T. Abe, K. Watanabe, J. Alloys Comp., 334, 232 (2002).

[6] T. Abe, S. Inoue, D. Mu, Y. Hatano, K. Watanabe. J. Alloys Comp., 349, 279 (2003).

[7] G. Mulas, L. Schiffini, G. Cocco, J. Mater. Res., 119, 3279 (2004).

[8] N. Cui, J.L. Luo, J. Alloys Comp., 265, 305 (1998).

[9] L.B. Wang, J.B. Wang, H.T. Yuan, Y.J. Wang, Q.D. Li, J. Alloys Comp., 385, 304 (2004).

[10] S.G. Zhang, K. Yorimitsu, S. Nohara, T. Morikawa, H. Inoue, C. Iwakura, J. Alloys Comp., 270, 123 (1998).

[11] S. Ruggeri, L. Roue, G.X. Liang, J. Huot, R. Schulz, J. Alloys Comp., 343, 170 (2002).

[12] M. Jurczyk, L. Smardz, A. Szajek, Mater. Sci. Eng. B 108, 67 (2004).

[13] C. Rongeat, L. Roué, J. Power Sources, 132, 302 (2004).

[14] P.H.L. Notten, P. Hokkeling, J. Electrochem. Soc., 138, 1877 (1991).

[15] H. Ye, H. Zhang, J.X. Cheng, T.S. Huang, J. Alloys Comp., 308, 163 (2000).

[16] Y. Fukumoto, M. Miyamoto, M. Matsuoka, C. Iwakura, Electrochim. Acta., 40, 845 (1995).

[17] H. Inoue, H. Iden, R. Shinya, S. Nohara, C. Iwakura, J. Electrochem. Soc., 151, A939 (2004).

[18] H. Senoh, M. Ueda, H. Inoue, N. Furukawa, C. Iwakura, J. Alloys Comp., 266, 111 (1998).

[19] S. Nohara, N. Fujita, S.G. Zhang, H. Inoue, C. Iwakura, J. Alloys Comp., 267, 76 (1998).

[20] S.G. Zhang, Y. Hara, T. Morikawa, H. Inoue, C. Iwakura, J. Alloys Comp., 293-295, 552 (1999).

[21] S.S. Han, H.Y. Lee, N.H. Goo, W.T. Jeong, K.S. Lee, J. Alloys Comp., 330–332, 841 (2002).

[22] L.Q. Li, I. Saita, K. Saito, T. Akiyama, Intermetallics, 10, 927 (2002).

[23] Z.X. Yu, Z.Y. Liu, E.D. Wang, Mater. Sci. Eng.A, 335, 43 (2002).

[24] G. Liang, S. Boily, J. Huot, A. Van Neste, R. Schulz, Mater. Sci. Forum, 267–272, 1049 (1998).

[25] B. Liao, Y.Q. Lei, L.X. Chen, G.L. Lu, H.G. Pan, Q.D. Wang, J. Alloys Comp., 376, 186 (2004).

[26] H.T. Yuan, E.D. Yang , H.B. Yang, B. Liu, L.B. Wang, R. Cao, Y.S. Zhang, J. Alloys Comp., 291, 244 (1999).

[27] Y.Q. Lei, Y.M. Wu, Q.M. Yang, J. Wu, Q.D. Wang, Z. Phys. Chem. 183, 1419 (1994).

[28] T.J. Ma, Y. Hatano, T. Abe, K. Watanabe, J. Alloys Comp., 391, 313 (2005).

[29] M.W. Meng, X.Y. Liu, J. Cheng, H.Y. Zhou, J. Alloys Comp., 372, 285 (2004).

[30] M. Pasturel, J.L. Bobet, B. Chevalier, J. Alloys Comp., 356–357, 764 (2003).

[31] N. Cui, J.L. Luo, K.T. Chuang, J. Alloys Comp., 302, 218 (2000).

[32] J.L. Luo, N. Cui, J. Alloys Comp., 264, 299 (1998).

[33] A.J. Bard, L.R. Faulkner, "Electrochemical Methods: Fundamentals and Applications", Wiley, New York, 1980.

[34] T. Vogt, J.J. Reilly, J.R. Johnson, G.D. Adzic, J. McBreen, J. Electrochem. Soc., 146, 15 (1999).

[35] B.N. Popov, G. Zheng, R.E. White, J. Appl. Electrochem., 26, 603 (1996).